Micropolar fluid flow through a stenosed bifurcated artery

Darbhasayanam Srinivasacharya, Gade Madhava Rao

Department of Mathematics, National Institute of Technology,
Warangal, Telangana-506004, India
dsc@nitw.ac.in; dsrinivasacharya@yahoo.com

Abstract. The aim of this article is to investigate the blood flow in bifurcated artery with mild stenosis taking blood as a micropolar fluid. The arteries forming bifurcation are taken to be symmetric and straight cylinders of finite length. The governing equations are non-dimensionalized, and coordinate transformation is used to convert the irregular boundary to a regular boundary. The resulting system of equations is solved numerically using the finite difference method. The variation of velocity, microrotation, shear stress, flow rate and impedance near the flow divider with relevant physical parameters are presented graphically. It is found that, due to backflow and secondary flow, impedance and flow rate are perturbed largely at the apex. It is also seen that the microrotation changes its sign from negative to positive for increase values of bifurcated angle and micropolar coupling number.

Keywords: micropolar fluid, bifurcated artery, stenosis, shear stress, impedance.

1 Introduction

Fluid dynamical aspects of many biological systems and the human cardiovascular system have gained much attention in recent years. One of the most frequently occurring abnormalities in the cardiovascular system of human beings is atherosclerosis. Atherosclerotic constriction in the arterial system is known as arterial stenosis. Local hemodynamics particularly in and around stenoses are believed to play an important role in cardiovascular disease. It is a fact that at different locations in the arterial system, may form and grow stenosis due to abnormal intravascular development. If this disease takes a severe form, it may lead to stroke, heart attack and various cardiovascular diseases. The effect of abnormal growth in arteries (stenosis) on the cardiovascular system has been found by studying the flow characteristics of blood in the stenosed artery. The initiation of atherosclerotic plaque is more likely to be dependent on the geometry of the arteries. The

curvatures, junctions and bifurcations of large and medium arteries are severely affected by atherosclerosis. Several researchers have reported the blood flow through arterial bifurcation in view of its importance in the genesis and diagnosis of atherosclerosis.

To investigate the correlation between atherosclerosis and blood flow dynamics in the carotid artery, the blood was assumed as an incompressible Newtonian fluid and simulated using computational fluid dynamics. It is well known that blood, being a suspension of cells, behaves like a non-Newtonian fluid at low shear rates and during its flow through narrow blood vessels. Chakravarty and Sen [4] studied to demonstrate the effects of constricted flow characteristics and the wall motion on the wall shear stress, on the concentration profile and on the mass transfer. Chen and Lu [5] investigated the influence of the non-Newtonian properties of blood in the rigid model of the carotid bifurcation under pulsatile flow condition. Shaw et al. [20] presented effect of shear stress with bifurcated angle, height of the stenosis and time both in femoral and coronary artery near the apex and outer wall of the boundary. Fan et al. [13] considered the pulsatile non-Newtonian flow in the carotid artery bifurcation and suggested that the flow behavior obtained by the Casson model had no difference when compared with the flow characterizations obtained by the Newtonian model. Gupta [14] investigated the flow field in the carotid artery considering fluid-structure interaction. Lee et al. [17] discussed the determination of the blood viscosity of non-Newtonian fluid using two constitutive models such as Casson and Herschel–Bulkley models and suggested that the Casson model is better than the Herschel–Bulkley model to represent the non-Newtonian characteristics of blood viscosity.

The micropolar fluids introduced by Eringen [12] exhibit some microscopic effects arising from the local structure and micro motion of the fluid elements. Further, they can sustain couple stresses. The model of micro polar fluid represents fluids consisting of rigid randomly oriented (or spherical) particles suspended in a viscous medium, where the deformation of the particles is ignored. The fluids containing certain additives, some polymeric fluids and animal blood are examples of micro polar fluids. Parvathamma and Devanathan [18] conisdered the pulsatile flow in tubes with and without longitudinal vibration using microcontinuum approach. Devanathan and Parvathamma [6] discussed the flow of micropolar fluid through a tube with stenosis and analyzed that the critical range of Reynolds number and wall shear stress are modified due to the micropolar fluids. Hogan and Henriksen [15] presented a micropolar model for blood flow through an idealized stenosis. Hogan and Henriksen [16] used finite element method to obtain numerical solution of differential equations of laminar flow of a fluid with microstructure. Abdullah and Amin [1] presented an analysis of blood flow through a single stenosis by considering a micropolar fluid model for blood flow. Shit and Roy [21] investigated the effect of externally imposed body acceleration and magnetic field on the pulsatile flow of blood through an arterial segment having stenosis. Srinivasacharya and Srikanth [22] reported that the flow patterns strongly depend on the geometry of stenosis. Sarifuddin et al. [19] developed a mathematical model of unsteady non-Newtonian blood flow together with heat transfer through constricted arteries. Ellahi et al. [8–11] studied the blood flow of micropolar fluid, Jeffrey fluid, Prandtl fluid and nanofluid through a tapered stenosed arteries. Ellahi et al. [7] analyzed the non-Newtonian micropolar fluid in arterial blood flow through composite stenosis. Akbar et al. [2] investigated the characteristics of blood

flow at the throat of stenosis, where blood is assumed as Williamson fluid flowing through stenosed arteries with permeable walls.

In the present study, the steady flow of an incompressible micropolar fluid through a bifurcated artery with mild stenosis is investigated. The variation of impedance and shearing stress is analyzed for various values of micropolar and geometric parameters.

2 Mathematical formulation

Consider a laminar and steady flow of incompressible blood through a bifurcated artery with mild stenosis in its lumen of parent artery. Blood is assumed to be a micropolar fluid of constant density. The stenosis over a length of the artery is assumed to have developed in an axi-symmetric manner, and the parent aorta have a single mild stenosis in its lumen. Let (r, θ, z) be the co-ordinates of the material point in a cylindrical polar co-ordinate system, of which z is taken as central axis of the parent artery. The arteries forming bifurcations are symmetrical about z-axis and are finite straight circular cylinders. Curvature is introduced at the lateral junction and the flow divider so that the possibility of the presence of any discontinuity leading to non-existent flow separation zones can be removed.

The equations governing the flow of laminar, steady, incompressible and micropolar fluid in the absence of body force and body couple are

$$\nabla \cdot \overline{q} = 0, \tag{1}$$

$$\rho(\overline{q} \cdot \nabla)\overline{q} = -\nabla p + \kappa \nabla \times \overline{\nu} - (\mu + \kappa)\nabla \times \nabla \times \overline{q}, \tag{2}$$

$$\rho j(\overline{q} \cdot \nabla)\overline{\nu} = -2k\overline{\nu} + \kappa \nabla \times \overline{q} - \gamma \nabla \times \nabla \times \overline{\nu} + (\alpha_1 + \beta_1 + \gamma)\nabla(\nabla \cdot \overline{\nu}), \tag{3}$$

where $\overline{q}$ is the velocity vector, $\overline{\nu}$ is the microrotation vector and p is the fluid pressure, ρ and j are the density and microgyration parameter of the fluid. Also, the material constants μ, κ, α_1, β_1 and γ satisfy the following inequalities:

$$\kappa \geqslant 0, \qquad 2\mu + \kappa \geqslant 0, \qquad 3\alpha_1 + \beta_1 + \gamma \geqslant 0, \qquad \gamma \geqslant |\beta_1|. \tag{4}$$

The geometry of the bifurcated artery with stenosis in its parent artery with outer and inner walls described by Chakravarty and Mandal [3] as follows:

$$R_1(z) = \begin{cases} a, & 0 \leqslant z \leqslant d', \\ a - \frac{4\tau_m}{l_0^2}(l_0(z - d') - (z - d')^2), & d' \leqslant z \leqslant d' + l_0, \\ a, & d' + l_0 \leqslant z \leqslant z_1, \\ a + r_0 - \sqrt{r_0^2 - (z - z_1)^2}, & z_1 \leqslant z \leqslant z_2, \\ 2r_1 \sec \beta + (z - z_2)\tan \beta, & z_2 \leqslant z \leqslant z_{\max}, \end{cases} \tag{5}$$

$$R_2(z) = \begin{cases} 0, & 0 \leqslant z \leqslant z_3, \\ \sqrt{(r_0')^2 - (z - z_3 - r_0')^2}, & z_3 \leqslant z \leqslant z_3 + r_0'(1 - \sin \beta), \\ r_0' \cos \beta + z_4, & z_3 + r_0'(1 - \sin \beta) \leqslant z \leqslant z_{\max}, \end{cases} \tag{6}$$
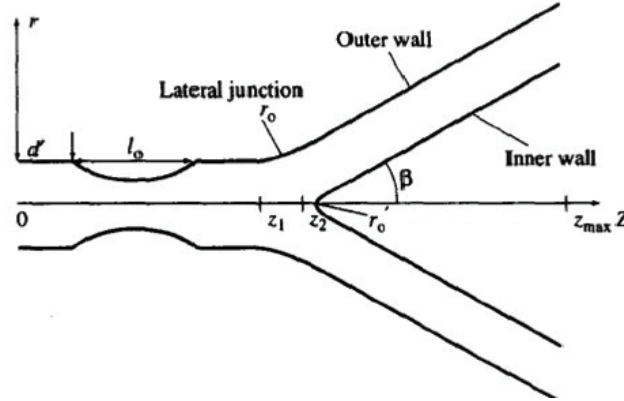
Figure 1. Schematic diagram of stenosed bifurcated artery.

where $R_1(z)$ is the radius of the outer wall, $R_2(z)$ is the radius of the inner wall, a is the radius of the parent artery in non-stenosed portion, r_1 is the radius of the daughter artery, r_0 is the radius of curvatures for the lateral junction, r_0' is the radius of curvatures for the flow divider, l_0 is the length of the stenosis at a distance d' from the origin, z_1 is the location of the onset of the lateral junction, z_2 is the offset of the lateral junction, z_3 is the apex, β is the half the bifurcation angle, τ_m represents the maximum height of the stenosis at $z = d' + l_0/2$ and $z_{\max}$ designates the finite length of the bifurcated artery under consideration.

The radii of curvature at the lateral junction and the flow divider are r_0 and r_0' given by

$$r_0 = \frac{a - 2r_1 \sec \beta}{\cos \beta - 1} \quad \text{and} \quad r_0' = \frac{(z_3 - z_2) \sin \beta}{1 - \sin \beta}, \tag{7}$$

where z_2, z_3 and z_4 lie on the axis of the bifurcated artery, which are functions of the half of bifurcated angle and are defined as

$$z_2 = z_1 + r_0 \sin \beta, \qquad z_3 = z_2 + q_1,$$

$$z_4 = \bigl(z - z_3 - r_0'(1 - \sin \beta)\bigr) \tan \beta,$$

where q_1 is a small number lying in between 0.1 and 0.5, this is defined for compatibility of the geometry.

Since the flow is axi-symmetric, all the variables are independent of θ. Hence, for this flow, the velocity is given by $\overline{q} = (u(r, z), 0, w(r, z))$ and the microrotation vector is $\overline{\nu} = (0, \nu(r, z), 0)$. With the assumption that the radial velocity is negligibly small and can be neglected for a low Reynolds number flow in a artery with mild stenosis (which implies that the variation of all the flow characteristics except pressure along the axial direction is negligible) [22], equations (1)–(3) can be written as

$$\frac{\partial p}{\partial r} = 0, \tag{8}$$

$$-\frac{\partial p}{\partial z} + \frac{\kappa}{r}\frac{\partial}{\partial r}(r\nu) + (\mu+\kappa)\frac{1}{r}\frac{\partial}{\partial r}\left(r\frac{\partial w}{\partial r}\right) = 0, \tag{9}$$

$$-2k\nu - \kappa\frac{\partial w}{\partial r} + \gamma\frac{\partial}{\partial r}\left(\frac{1}{r}\frac{\partial}{\partial r}(r\nu)\right) = 0. \tag{10}$$

The non-dimensional variables are defined as

$$r = a\widetilde{r}, \qquad r_1 = a\widetilde{r}_1, \qquad z = L\widetilde{z}, \qquad z_1 = a\widetilde{z}_1,$$

$$j = a^2, \qquad w = w_0\widetilde{w}, \qquad p = \frac{Lw_0\mu\widetilde{p}}{a^2}, \qquad \nu = \frac{w_0\widetilde{\nu}}{a}, \tag{11}$$

$$d = L\widetilde{d}, \qquad R_1(z) = a\widetilde{R}_1(\widetilde{z}), \qquad R_2(z) = a\widetilde{R}_2(\widetilde{z}),$$

where w_0 is characteristic velocity and L is characteristic length.

Introducing the non-dimensional variables (11) into equations (5)–(10) and dropping tildes, we get

$$R_1(z) = \begin{cases} 1, & 0 \leqslant z \leqslant d', \\ 1 - \frac{4\tau_m}{al_0^2}(l_0(z-d') - (z-d')^2), & d' \leqslant z \leqslant d' + l_0, \\ 1, & d' + l_0 \leqslant z \leqslant z_1, \\ 1 + r_0 - \sqrt{r_0^2 - (z-z_1)^2}, & z_1 \leqslant z \leqslant z_2, \\ 2r_1 \sec\beta + (z-z_2)\tan\beta, & z_2 \leqslant z \leqslant z_{\max}, \end{cases} \tag{12}$$

$$R_2(z) = \begin{cases} 0, & 0 \leqslant z \leqslant z_3, \\ \sqrt{(r_0')^2 - (z - z_3 - r_0')^2}, & z_3 \leqslant z \leqslant z_3 + r_0'(1 - \sin\beta), \\ r_0'\cos\beta + z_4, & z_3 + r_0'(1 - \sin\beta) \leqslant z \leqslant z_{\max}, \end{cases} \tag{13}$$

$$-\frac{\partial p}{\partial z} + \frac{N}{1-N}\frac{1}{r}\frac{\partial}{\partial r}(r\nu) + \frac{1}{1-N}\frac{1}{r}\frac{\partial}{\partial r}\left(r\frac{\partial w}{\partial r}\right) = 0, \tag{14}$$

$$-2\nu - \frac{\partial w}{\partial r} + \frac{2-N}{m^2}\frac{\partial}{\partial r}\left(\frac{1}{r}\frac{\partial}{\partial r}(r\nu)\right) = 0, \tag{15}$$

where $N = \kappa/(\mu+\kappa)$ is the coupling number ($0 \leqslant N \leqslant 1$) and $m^2 = a^2\kappa \times (2\mu+\kappa)/(\gamma(\mu+\kappa))$ is the micropolar parameter. It is to be noted from (14) and (15) that, when $N \to 0$ and $m \to \infty$ (i.e. $\kappa \to 0$ and $\gamma \to 0$), the system of equations represents to a classical Newtonian fluid model.

The non-dimensional boundary conditions are

$$\begin{aligned} \frac{\partial w}{\partial r} &= 0, & \nu &= 0 & &\text{on } r = 0 \text{ for } 0 \leqslant z \leqslant z_3, \\ w &= 0, & \nu &= 0 & &\text{on } r = R_1(z) \text{ for all } z, \\ w &= 0, & \nu &= 0 & &\text{on } r = R_2(z) \text{ for } z_3 \leqslant z \leqslant z_{\max}. \end{aligned} \tag{16}$$

The effect of $R_1(z)$ and $R_2(z)$ from the boundary conditions can be transferred into the governing equations by the following radial coordinate transformation [21]:

$$\xi = \frac{r - R_2}{R},\tag{17}$$

where $R(z) = R_1(z) - R_2(z)$,

Using this transformation in equations (14) and (15), they take the form

$$-\frac{\partial p}{\partial z} + \frac{N}{1 - N}\left(\frac{1}{R}\frac{\partial \nu}{\partial \xi} + \frac{\nu}{\xi R + R_2}\right) + \frac{1}{(1 - N)R^2}\frac{\partial^2 w}{\partial \xi^2}$$
$$+ \frac{1}{(1 - N)R(\xi R + R_2)}\frac{\partial w}{\partial \xi} = 0,\tag{18}$$

$$-\frac{1}{R}\frac{\partial w}{\partial \xi} + \frac{2 - N}{m^2 R^2}\frac{\partial^2 \nu}{\partial \xi^2} - \left(2 + \frac{2 - N}{m^2(\xi R + R_2)^2}\right)\nu + \frac{(2 - N)}{m^2 R(\xi R + R_2)}\frac{\partial \nu}{\partial \xi} = 0,\tag{19}$$

and the boundary conditions (16) are transformed to the form

$$\begin{aligned}
\frac{\partial w}{\partial \xi} &= 0, & \nu &= 0 & \text{on } \xi = 0 \text{ for } 0 \leqslant z \leqslant z_3,\\
w &= 0, & \nu &= 0 & \text{on } \xi = 1 \text{ for all } z,\\
w &= 0, & \nu &= 0 & \text{on } \xi = 0 \text{ for } z_3 \leqslant z \leqslant z_{\max}.
\end{aligned}\tag{20}$$

3 Method of solution

The reduced equations (18) and (19) along with the boundary conditions (20) are solved numerically using finite-difference method. A two dimensional computational grid is imposed in z, ξ-plane. The stepping process is defined by $z_i = i\Delta z$, $i = 0, 1, \ldots, n$, and $\xi_j = j\Delta\xi$, $j = 0, 1, \ldots, J$, where Δz and $\Delta\xi$ are step lengths in the axial and radial directions, respectively. If $w_{i,j}$ represents the value of the variable w at (z_i, ξ_j), then the derivatives are replaced by central difference approximations

$$\begin{aligned}
\frac{\partial w}{\partial \xi} &= \frac{w_{i,j+1} - w_{i,j-1}}{2\Delta\xi}, & \frac{\partial^2 w}{\partial \xi^2} &= \frac{w_{i,j+1} - 2w_{i,j} + w_{i,j+1}}{(\Delta\xi)^2},\\
\frac{\partial \nu}{\partial \xi} &= \frac{\nu_{i,j+1} - \nu_{i,j-1}}{2\Delta\xi}, & \frac{\partial^2 \nu}{\partial \xi^2} &= \frac{\nu_{i,j+1} - 2\nu_{i,j} + \nu_{i,j-1}}{(\Delta\xi)^2}.
\end{aligned}\tag{21}$$

Substituting (21) in (18) and (19), we get the following system of equations:

$$\left[\frac{\xi_j R_i + R_{2i}}{(\Delta\xi)^2} - \frac{R_i}{2\Delta\xi}\right]w_{i,j-1} - \frac{2(\xi_j R_i + R_{2i})}{(\Delta\xi)^2}w_{i,j} + \left[\frac{\xi_j R_i + R_2}{(\Delta\xi)^2} + \frac{R_i}{2\Delta\xi}\right]w_{i,j+1}$$
$$- \frac{N R_i(\xi_j R_i + R_{2i})}{2\Delta\xi}\nu_{i,j-1} + N R_i^2 \nu_{i,j} + \frac{N R_i(\xi_j R_i + R_{2i})}{2\Delta\xi}\nu_{i,j+1}$$
$$= R_i^2(1 - N)(\xi_j R_i + R_{2i})\frac{\mathrm{d}p}{\mathrm{d}z},\tag{22}$$

$$\frac{w_{i,j-1} - w_{i,j+1}}{2\Delta\xi} + \frac{2-N}{m^2}\left[\frac{1}{R_i(\Delta\xi)^2} - \frac{1}{2(\Delta\xi)(\xi_j R_i + R_{2i})}\right]\nu_{i,j-1}$$
$$-\left[2R_i + \frac{2-N}{m^2}\left(\frac{2}{R_i(\Delta\xi)^2} + \frac{R_i}{(\xi_j R_i + R_{2i})^2}\right)\right]\nu_{i,j}$$
$$+\frac{2-N}{m^2}\left[\frac{1}{R_i(\Delta\xi)^2} + \frac{1}{2(\Delta\xi)(\xi_j R_i + R_{2i})}\right]\nu_{i,j+1} = 0. \tag{23}$$

The boundary conditions (20) reduce to

$$w_{i,1} = w_{i,2} \quad \text{and} \quad \nu_{i,1} = 0 \quad \text{for } z < z_3,$$
$$w_{i,J+1} = 0 \quad \text{and} \quad \nu_{i,J+1} = 0 \quad \text{for all } i,$$
$$w_{i,1} = 0, \quad \text{and} \quad \nu_{i,1} = 0 \quad \text{for } z \geqslant z_3.$$

Equations (22)–(23) results in a block-tridiagonal matrix and is solved by block elimination method.

The physical quantities of interest are the flow rate, impedance and shear stress for both parent and daughter arteries. The flow rate for both parent and daughter arteries is determined using

$$Q_p = 2\pi R_i\left[R_i\int_0^1 \xi_i w_{i,j}\,\mathrm{d}\xi_i + R_{2i}\int_0^1 w_{i,j}\,\mathrm{d}\xi_i\right]$$

and

$$Q_d = \pi R_i\left[R_i\int_0^1 \xi_i w_{i,j}\,\mathrm{d}\xi_i + R_{2i}\int_0^1 w_{i,j}\,\mathrm{d}\xi_i\right].$$

The resistance to the flow (resistive impedance) in parent and daughter artery is calculated using

$$(\lambda_p)_i = \left|\frac{z_3}{Q_p}\right| \quad \text{for } z < z_3, \qquad (\lambda_d)_i = \left|\frac{(z_{\max} - z_3)}{Q_d}\frac{\mathrm{d}p}{\mathrm{d}z}\right| \quad \text{for } z \geqslant z_3.$$

The wall shear stress is given by

$$\tau = \frac{1}{1-N}\frac{\mathrm{d}w}{\mathrm{d}r} + \frac{N}{1-N}\nu.$$

This wall shear stress is calculated at the parent outer wall ($r = R_1(z)$) and the daughter inner wall ($r = R_2(z)$) of the bifurcated artery, respectively.

4 Results and discussion

In order to validate the accuracy of our method, we have compared the results of velocity and microrotation with the analytical solution of Eringen [12] in the absence of τ_m, $R_2(z)$, r_0 and β as a special case by taking $N = 0.75$, $m = 10$, $r_1 = 0.5$ and $\mathrm{d}p/\mathrm{d}z = 2$. The comparison in the above case is found to be in good agreement as shown in Table 1.

Table 1. Comparison analysis for the velocity and microrotation calculated by the present method and that of analytical solution [12] for $N = 0.75$, $m = 10$, $\mathrm{d}p/\mathrm{d}z = 2$, $R(z) = 1$ and $R_2(z) = 0$.

	Velocity		Microrotation	
ξ	Analytical solution [12]	Present	Analytical solution [12]	Present
0	0.1311	0.1312	0	0
0.1	0.1297	0.1298	0.0032	0.0032
0.2	0.1257	0.1258	0.0062	0.0062
0.3	0.1188	0.1188	0.0088	0.0088
0.4	0.1094	0.1094	0.0109	0.0109
0.5	0.0972	0.0973	0.0122	0.0122
0.6	0.0826	0.0826	0.0126	0.0126
0.7	0.0654	0.0654	0.0118	0.0118
0.8	0.0458	0.0458	0.0096	0.0096
0.9	0.0239	0.0239	0.0057	0.0057
1.0	0	0	0	0

To have a better understanding of the flow characteristics, numerical results for the velocity, microrotation, flow rate, shear stress and impedance are calculated for different values of parameters by taking $a = 5$ mm, $d' = 10$ mm, $l_0 = 5$ mm, $\beta = \pi/10$, $m = 10$, $r_1 = 0.51a$, $\tau_m = 2a$.

Figure 2 depicts the variation of velocity and microrotation profiles with N at maximum height of the stenosis in the parent artery. It is seen from Fig. 2 that the velocity decreases with increase of N. Since in the limit $N \to 0$, equations (3) and (4) reduce to the corresponding relations for a viscous fluid, the velocity in case of micropolar fluid is less than that of viscous fluid. This implies that the streaming blood velocity increases with decrease in values of blood viscosity. From Fig. 2, it is evident that the microrotation decrease with the increase of coupling number N.

The effect of N on the velocity and the microrotation in the daughter artery at $z = 22.5$ is illustrated through Fig. 3. It is noticed from Fig. 3(a) that the velocity decreases with the increase of N. It is observed from Fig. 3(b) that the microrotation changes its sign as ξ varies from 0 to 1. As N increases, the microrotation increases near the inner wall $\xi = 0$ of the artery, becomes zero at the center of the artery and then decreases near the outer wall $\xi = 1$ of the artery.

The influence of β on the axial velocity and microrotation in the daughter artery at $z = 22.5$ is presented in Fig. 4. The axial velocity increases with increasing values of β. The maximum of the velocity shifts towards the inner wall of the artery. As β increases, the microrotation decreases near the inner wall $\xi = 0$ of the artery, becomes zero at the center of the artery and then increases near the outer wall $\xi = 1$ of the artery.

The variations of shear stress along the inner and the outer walls of the daughter artery with β is illustrated through Figs. 5(a) and 5(b), respectively. It is found from Fig. 5(a) that the shear stress decreases with increase in the values of β along the inner wall of the daughter artery. It is observed from Fig. 5(b) that the shear stress increases with increase in the values of β along the outer wall of the daughter artery.
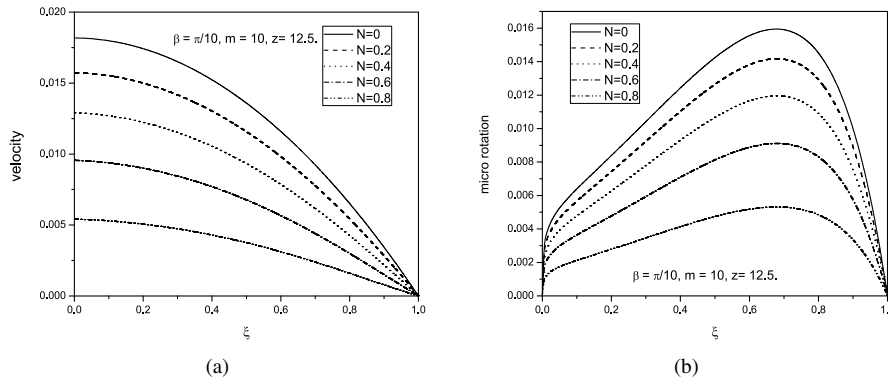
Figure 2. Profiles of (a) velocity and (b) microrotation in parent artery at $z = 12.5$ for different values of N and fixed values of $\beta = \pi/10$, $m = 10$.
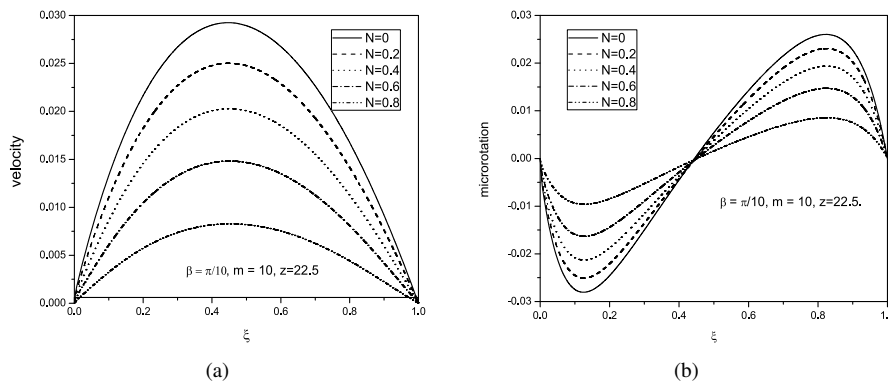

Figure 3. Profiles of (a) velocity and (b) microrotation in daughter artery at $z = 22.5$ for different values of N and fixed values of $\beta = \pi/10$, $m = 10$.
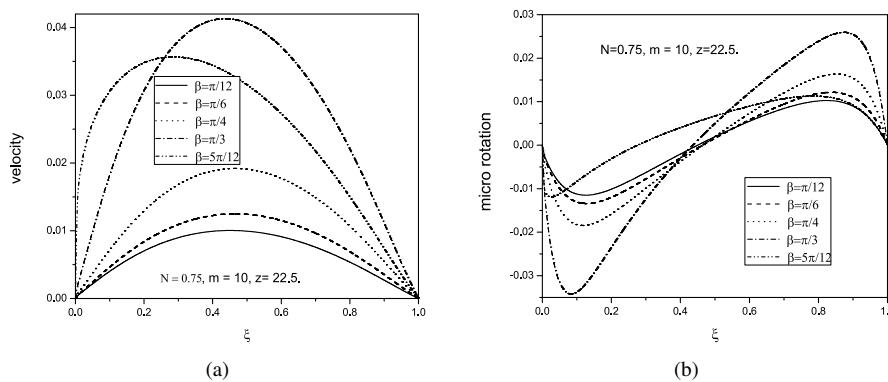

Figure 4. Profiles of (a) velocity and (b) microrotation in daughter artery at $z = 22.5$ for different values of β and fixed values of $N = 0.75$, $m = 10$.
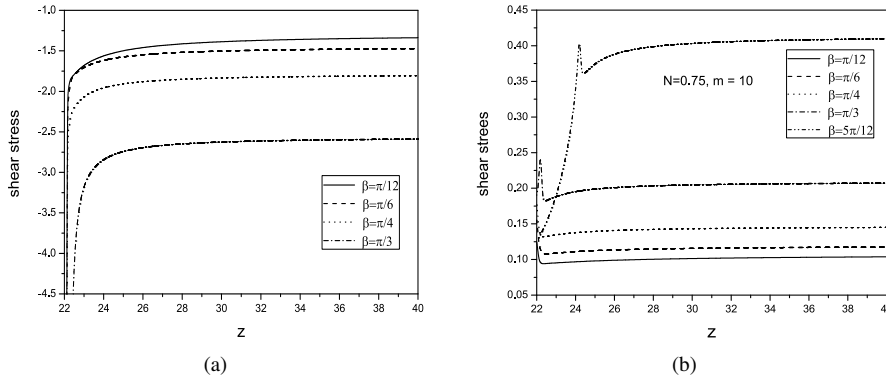
Figure 5. Effect of half of the bifurcated angle along (a) inner, (b) outer walls of the daughter with $N = 0.75$, $m = 10$ on shear stress.
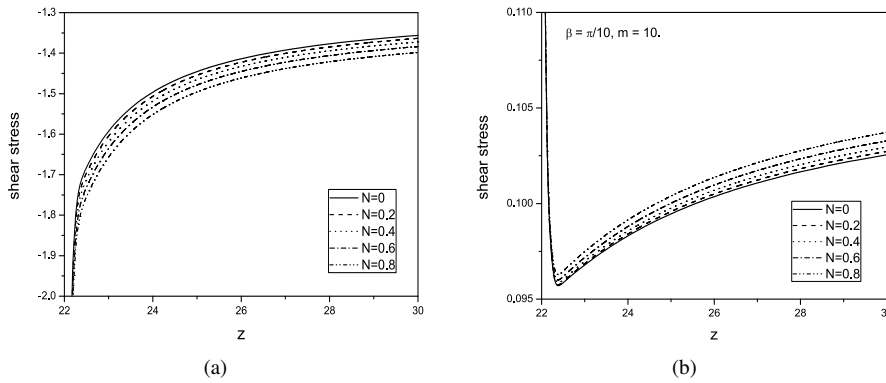

Figure 6. Effect of coupling number N along (a) inner, (b) outer walls of the daughter with $\beta = \pi/10$, $m = 10$ on shear stress.
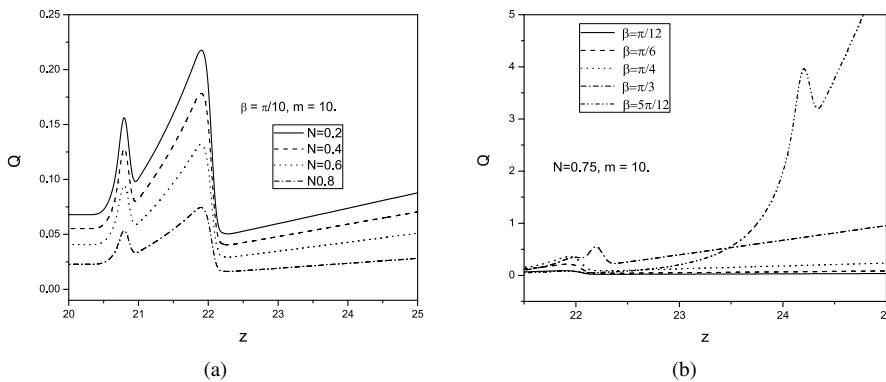

Figure 7. Effect of (a) coupling number N with $\beta = \pi/10$, $m = 10$; (b) β with $N = 0.75$, $m = 10$ on volumetric flow rate.
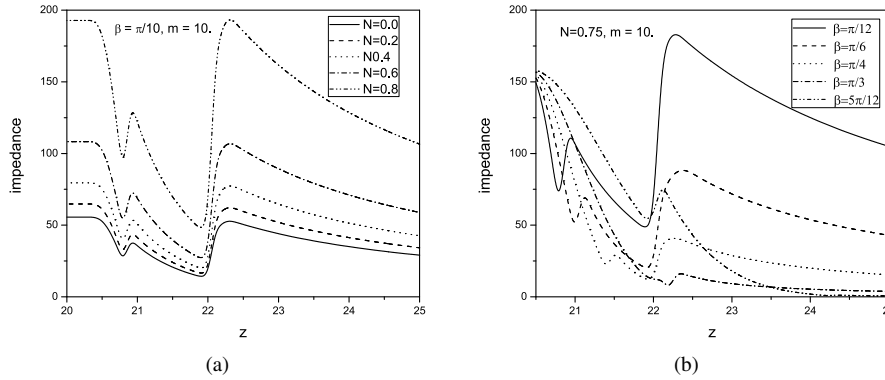
Figure 8. Effect of (a) coupling number N with $\beta = \pi/10$, $m = 10$; (b) β with $N = 0.75$, $m = 10$ on impedance.

The effect of N on shear stress along the inner and outer walls of the daughter artery is shown in Figs. 6(a) and 6(b), respectively. As the value of N increases, the shear stress decreases along the inner wall and increases along the outer wall of the daughter artery.

The variations of volumetric flow rate along the axial direction with N and β on both sides of apex are depicted in Figs. 7(a) and 7(b). Flow rate decreases with an increase in the values of N. But, due to the presence of backflow near the curvature of the diverging outer wall, flow rate increases till inset of lateral junction, then a small decrease is identified and then increases up to the apex. Thereafter, flow rate is uniform till z_{max}. Flow rate increases with increasing values of β.

The variation of impedance with N and β is presented in Figs. 8(a) and 8(b). Impedance increases with decreasing values of N. In general, it is noticed that the impedance decreases with an increase in the value of z up to lateral junction, then a slight increase occurs suddenly, and after that gradually decreases till the apex, and then a sudden increase is identified. This is because of diverging of blood flow at bifurcation of the artery. Thereafter, it is found that the impedance is uniform till z_{max}. The same trend is observed with β.

5 Conclusions

The present investigation helps us to understand numerically the influence of N and β on velocity, microrotation, flow rate, shear stress and impedance of streaming blood flow through a bifurcated artery with mild stenosis treating blood as micropolar fluid.

- In daughter artery, velocity decreases with increasing values of N whereas it increases with increasing values of β. The microrotation changes its sign to increase values of N and β.
- As N and β increases, the shear stress decreases at the inner wall and increases at the outer wall of the daughter artery.

- On both sides of the apex, flow rate decreases with increasing values of N whereas it increases with increase of β.
- Impedance increases with an increase in the values of N and decreases with increase of β.

References

1. I. Abdullah, A. Amin, A micropolar fluid model of blood flow through a tapered artery with a stenosis, *Math. Methods Appl. Sci.*, **33**:1910–1923, 2010.

2. N.S. Akbar, S.U. Rahman, R. Ellahi, S. Nadeem, Blood flow study of Williamson fluid through stenosed arteries with permeable walls, *Eur. Phys. J. Plus*, **129**, 2014.

3. S. Chakravarty, P.K. Mandal, An analysis of pulsatile flow in a model aortic bifurcation, *Int. J. Eng. Sci*, **35**(4):409–422, 1997.

4. S. Chakravarty, S. Sen, A mathematical model of blood flow and convective diffusion processes in constricted bifurcated arteries, *Korea–Australia Rheology Journal*, **18**(2):51–65, 2006.

5. J. Chen, X.Y. Lu., Numerical investigation of the non-Newtonian pulsatile blood flow in a bifurcation model with a non-planar branch, *J. Biomech.*, **39**:818–832, 2006.

6. R. Devanathan, S. Parvathamma, Flow of micropolar fluid through a tube with stenosis, *Med. Biol. Eng. Comput.*, **21**:438–445, 1983.

7. R. Ellahi, S.U. Rahman, G.M. Mudassar, S. Nadeem, K. Vafai, A mathematical study of non-Newtonian micropolar fluid in arterial blood flow through composite stenosis, *Appl. Math. Inf. Sci.*, **8**(4):1567–1573, 2014.

8. R. Ellahi, S.U. Rahman, S. Nadeem, Blood flow of Jeffrey fluid in a catherized tapered artery with the suspension of nanoparticles, *Phys. Lett. A*, **378**:2973–2980, 2014.

9. R. Ellahi, S.U. Rahman, S. Nadeem, N.S. Akbar, Blood flow of nanofluid through an artery with composite stenosis and permeable walls, *Appl. Nanosci.*, **4**:919–926, 2014.

10. R. Ellahi, S.U. Rahman, S. Nadeem, S. Akbar, Influence of heat and mass transfer on micropolar fluid of blood flow through a tapered stenosed arteries with permeable walls, *J. Comput. Theor. Nanosci.*, **11**(4):1156–1163, 2014.

11. R. Ellahi, S.U. Rahman, S. Nadeem, K. Vafai, The blood flow of Prandtl fluid through a tapered stenosed arteries in permeable walls with magnetic fiel, *Commun. Theor. Phys*, **63**(3):353–358, 2015.

12. A.C. Eringen, Theory of micropolar fluids, *J. Math. Mech.*, **16**:1–16, 1966.

13. Y. Fan, W. Jiang, Y. Zou, J. Li, J. Chen, X. Deng, Numerical simulation of pulsatile non-Newtonian flow in the carotid artery bifurcation, *Acta Mech Sin.*, **25**:249–255, 2009.

14. A.K Gupta, Performance and analysis of blood flow through carotid artery, *Int. J. Eng. Bus. Manag.*, **3**:1–6, 2011.

15. H.A. Hogan, M. Henriksen, An evaluation of a micropolar model for blood flow through an idealized stenosis, *J. Biomech.*, **22**(3):211–218, 1989.

16. H.A. Hogan, M. Henriksen, A finite element formulation for laminar flow of a fluid with microstructure, *Int. J. Numer. Methods Fluids*, **13**:1267–1287, 1991.

17. B.K. Lee, S. Xue, J.H. Nam, H.J. Lim, S.H. Shin, Determination of blood viscosity and yield stress with a pressure-scanning capillary hemorheometer using constitutive models, *Korea–Australia Rheology Journal*, **23**:1–6, 2011.

18. S. Parvathamma, R. Devanathan, Microcontinuum approach to the pulsatile flow in tubes with and without longitudinal vibration, *Bull. Math. Biol.*, **45**(5):721–737, 1983.

19. Sarifuddin, S. Chakravarty, P.K. Mandal, Heat transfer to micropolar fluid flowing through an irregular arterial constriction, *Int. J. Heat Mass Transfer*, **56**:538–551, 2013.

20. S. Shaw, R.S.R. Gorla, P.V.S.N. Murthy, C.O. Ng, Pulsatile Casson fluid flow through a stenosed bifurcated artery, *Int. J. Fluid Mech. Res.*, **36**(1):43–63, 2009.

21. G.C. Shit, M. Roy, Pulsatile flow and heat transfer of a magneto-micropolar fluid through a stenosed artery under the influence of body acceleration, *Journal of Mechanics in Medicine and Biology*, **11**:643–661, 2011.

22. D. Srinivasacharya, D. Srikanth, Flow of micropolar fluid through catheterized artery – A mathematical model, *Int. J. Biomath.*, **5**(2):1250019, 2012.